The role of lithium iodide addition to lithium thiophosphate: Implications beyond conductivity

Nikhilendra Singh[†], James Horwath[‡], Patrick Bonnick[†], Koji Suto^{†1}, Eric Stach[‡], Tomoya Matsunaga^{†1}, John Muldoon[†] and Timothy S. Arthur^{*†}

†Toyota Research Institute of North America, 1555 Woodridge Ave, Ann Arbor, MI 48105

FSingh Center for Nanotechnology, 3231 Walnut Street, Philadelphia, PA 19104

Solid-state batteries, Interface, Operando Analysis

ABSTRACT: Due to their high conductivity and potential to utilize lithium metal, lithium thiophosphate electrolytes have attracted a lot of attention to realize solid-state batteries for vehicle applications. However, the lithium metal still presents many challenges, especially under limited-lithium conditions. Here, the interface between lithium thiophosphate and lithium iodide-doped lithium thiophosphate with the lithium metal has been investigated. Lithium iodide play a protective role at the interface and enables improved lithium cycling. *Operando* TEM analysis reveals that delamination and "dead lithium" at the interface as major challenges for solid-state batteries.

Energy Storage to enable the next generation of mobile devices, homes and transportation is pivotal to stem the movement into environmental tragedy. Batteries has long provided a means to enable mobility, and since the inception of Li-ion batteries in 1991, research has focused on finding materials, interfaces and processes to reliably and affordably introduce them into a range of devices. Solid-state batteries (SSB), where the liquid electrolyte and polymeric separator are replaced with a solid-state Li-ion conductor, are primed to accelerate the realization of practical devices. Safety, bi-polar stacking and lithium metal compatibility are the positive attributes claimed for SSB. ¹⁻³

The key driver for SSB is the conductivity of the solid-state electrolyte; playing the pivotal role of fast Li⁺-ion conductor while maintaining a robust electrical separation between the battery electrodes. Shao-horn *et al* has outlined the various materials, properties and conductivities that promote Li-ion flow and enable solid-state batteries.⁴ For decades, researchers have focused intently on incremental improvements in solid-state ion conductivity, with the seminal research on Li₁₀GeP₂S₁₂ by the Kanno *et al.* showing the possibility of solid-state conductivity to match organic, liquid electrolytes.^{5,} Indeed, lithium thiophosphates, such as crystalline agryodite phases and thio-lisicon glass-ceramics, have emerged as strong contenders to be applied to SSB due to the high conductivities and processability.⁷

One interesting avenue of research is the addition of lithium halides to lithium thiophosphates, which was first shown by Mercier et al to increase the conductivity of the Li₂S-P₂S₅ ceramic solid-electrolytes.8 Accessing high conductivity, without the addition of metal ions into the thiophosphate structure, is advantageous both from a resource management and reductive stability viewpoint. Tatsumisago et al. have recently highlighted the capability of LiI addition to Li₃PS₄ (LPS) to lower Young's Modulus and retain the mechanical integrity of the ceramic under volumetric changes and stresses of a silicon anode. Wang et al. found the addition of LiI improves critical current density (CCD) and cycle-life in symmetrical lithiummetal cells.¹⁰ The CCD is the current applied when lithium metal dendrite penetration is observed electrochemically. Additionally, Nitanii et al. have shown the increase in conductivity is related to thermal annealing conditions of LPS:0.5LiI, and a necessary step to further enhance the CCD of the solid-electrolyte. 11 Indeed, these results echo the work of Garcia-Mendez et al., showing the benefits of hot-pressing Li₃PS₄ to delay the onset of dendrite penetration.¹² Understanding the structural changes of LPS:0.5LiI has highlighted contribution of halide addition to the conductivity and CCD of the solid-electrolyte but has shed little light on the effect interface of between lithium metal and LPS:0.5LiI.

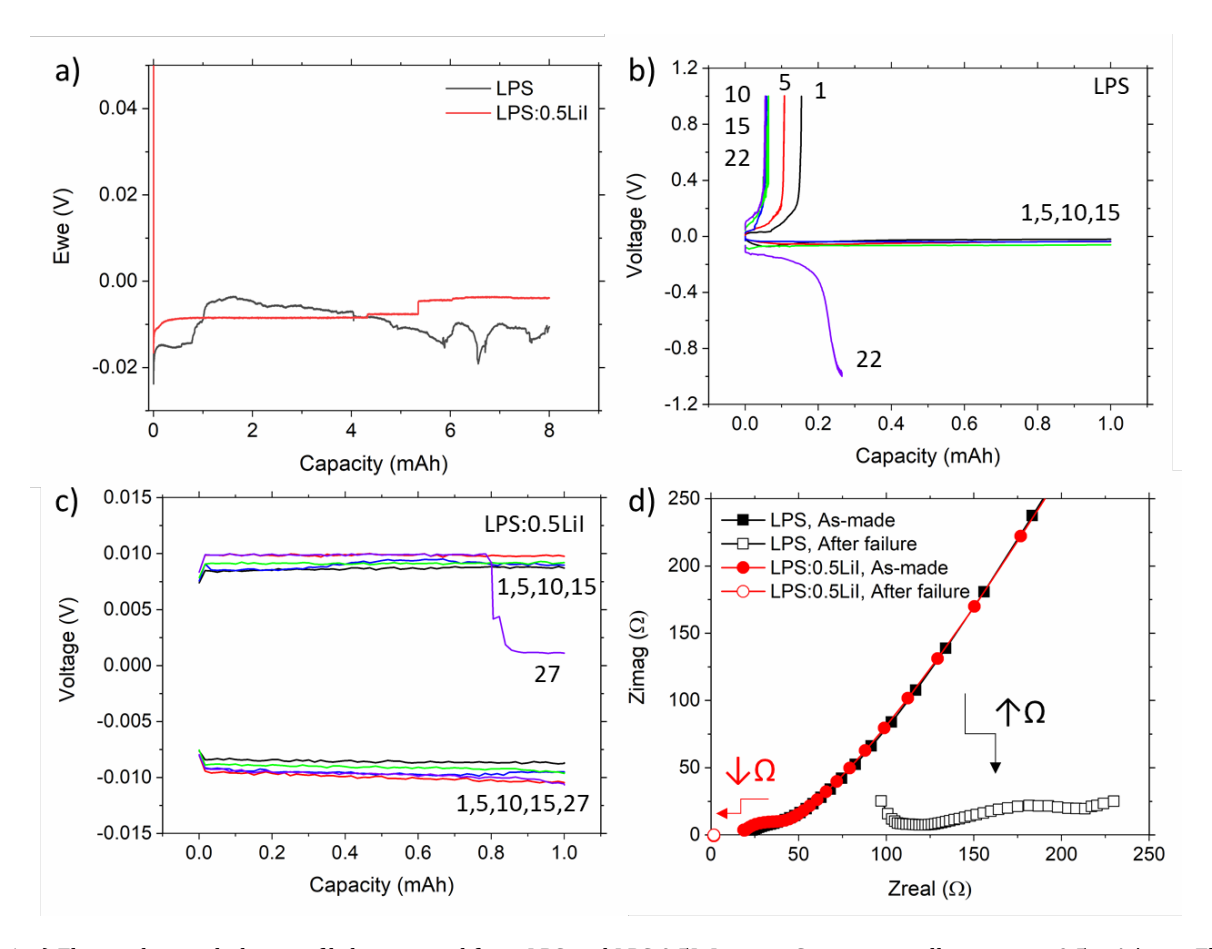


Figure 1. a) Electrochemical plating of lithium metal from LPS and LPS:0.5LiI onto a Cu current collector at j = 0.5 mA/cm². Electrochemical plating and stripping at 1 mA/cm² from b) LPS and c) LPS:0.5LiI. d) Electrochemical impedance spectra of LPS and LPS:0.5LiI as-made and after cycling failure.

In this study, we use advanced analytical techniques, such as operando electrochemical-transmission electron microscope (TEM) in the solid-state, scanning electron microscopy (SEM) and X-ray photoelectron spectroscopy (XPS), to understand the influence of LiI on the interface between Li-metal and LPS:0.5LiI. Through accessing the strengths afforded by these techniques, we show the presence of electrochemical interphases and their influence on the failure mechanisms of LPS and LPS:0.5LiI. The poor reductive stability of lithium thiophosphates into the decomposition products of Li₂S, Li₂S_x and Li₃P has been shown previously. ¹²⁻¹⁴ Due to the resistive, self-limiting nature of the interphase, researchers have contended that thiphosphates produce a working solid-electrolyte interphase. However, to our knowledge, repeated cycling under limited lithium conditions have not been pursued, and practical lithiummetal batteries rely on limiting the amount of lithium metal to enforce energy density calculations. 15 Additionally, the effect of iodine on the electrochemical interface must be determined.

The solution-based electrodeposition of metals has been extensively studied academically, as well as provided industrial solutions for practical devices. $^{16,\ 17}$ One interesting and applicable avenue of

research has been the use of surface-modifiers to affect the structure and morphology of deposited metals, for example surfactants, organic molecules and halide salts. In the liquid-based electrochemical deposition, iodine addition is well-known to influence the kinetics of crystallization and morphology of metal growth, and has been frequently been utilized to form compact, uniform films. Is-23 For solid-state electrodeposition, groups have shown the modification of lithium metal surfaces has significantly improved the galvanic cycling properties

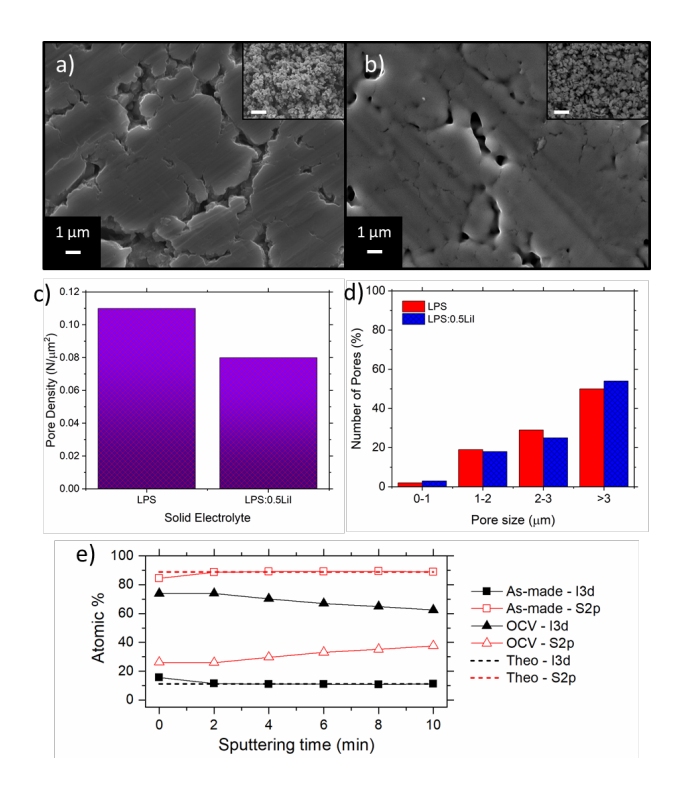


Figure 2. SEM images of pellet surfaces for a) LPS and b) LPS:0.5LiI (insets are as-made particles; scale bar 10 μm). c) Surface-pore density and d) pore-size analysis for the SE pellets. d) XPS depth-profiling analysis of a LPS:0.5LiI pellet asmade and after maintain OCV for 12 h in a Li-Li symmetrical cell.

using solid-state electrolytes, however, iodine adsorption has not been evidenced for the solid-state deposition of lithium metal, nor the influence on cell failure. Understanding the electrochemical interphase is a vital step to engineering practical SSB.

Results and Discussion

To maximize the energy of any battery system, capacity-matching between the anode and the cathode is critical. For the lithium metal anode, utilizing limited lithium metal, or ultimately a currently collector only, is advantageous to determine the practical lithium deposition/stripping efficiency and exclude the effect of a "lithium

metal reservoir". 15 Figure 1a) shows an electrochemical half-cell galvanic plating of lithium metal onto a copper current collector at j=0.25 mA cm⁻² at 60 °C, which is below the critical current density (CCD) of both LPS and LPS:0.5LiI.¹¹ The potential response to the deposition of 8 mAh cm⁻² (38.8 µm) of lithium metal from LPS fluctuates with time resulting is a "spiky" voltage profile. The change in voltage reflects the constant change in electrochemical surface area for deposition, rather than the penetration of a dendrite leading to an electrical short. Alternatively, the charge transfer resistance could increase due to the presence of Li₂S, Li₃P and Li₂S_x at the interface of deposition. In contrast, the potential response from LPS:0.5LiI is consistent and "smooth", barring small decreases in overpotential, which implies a uniform electrochemical deposition of metal onto the surface of copper. The presence of internal shorting was investigated through electrochemical impedance spectroscopy (EIS - Figure S1a), and the lack of an inductive loop provides evidence that the solid electrolyte remains as a barrier to electron flow between electrodes. After 8 mAh cm⁻² of Li-metal plating, the in situ generated Li-Li symmetric cell is galvanically cycled at 1 mA cm⁻² for 1 mAh (4.85 µm), as shown in Figure 1b) and c) for LPS and LPS:0.5LiI, respectively. The coulombic efficiency (CE) for lithium plating, described here as Q_{stripping} / Q_{plating}, is shown in Figure S1b for the first 20 cycles. LPS can only recover approximately 10 % while LPS:0.5LiI can recover 100 % of the reductive charge passed during plating. It must be noted that due to the excess of lithium plated during the first cycle, 100 % CE does not imply the complete stripping of all freshly deposited lithium metal, but rather the electrochemical oxidation of accessible lithium metal. Cell failure for the LPS electrolyte can be observed in Figure 1b during the 22nd cycle because of the inability to deposit 1 mAh cm⁻² worth of lithium during deposition. A trend of increasing resistance for LPS is reflected in the EIS (Figure 1d), where a $\sim 200 \ \Omega \ \text{cm}^{-2}$ increase in charge transfer resistance is responsible for the inability to plate lithium. LPS:0.5LiI, cell failure occurs when an internal short reduces the area specific resistance to $< 1 \Omega$ cm⁻² during the 27th cycle. presence of an inductive loop as well a singular real resistance value of 1.75 Ω cm⁻² is clear evidence of an internal short.

As previously reported, we conclude that the addition of LiI to LPS vastly improves the lithium metal cycling properties of the solid electrolyte. ^{10, 11, 24} Indeed, the addition of LiI shows a vast improvement in conductivity and activation energy. However, the

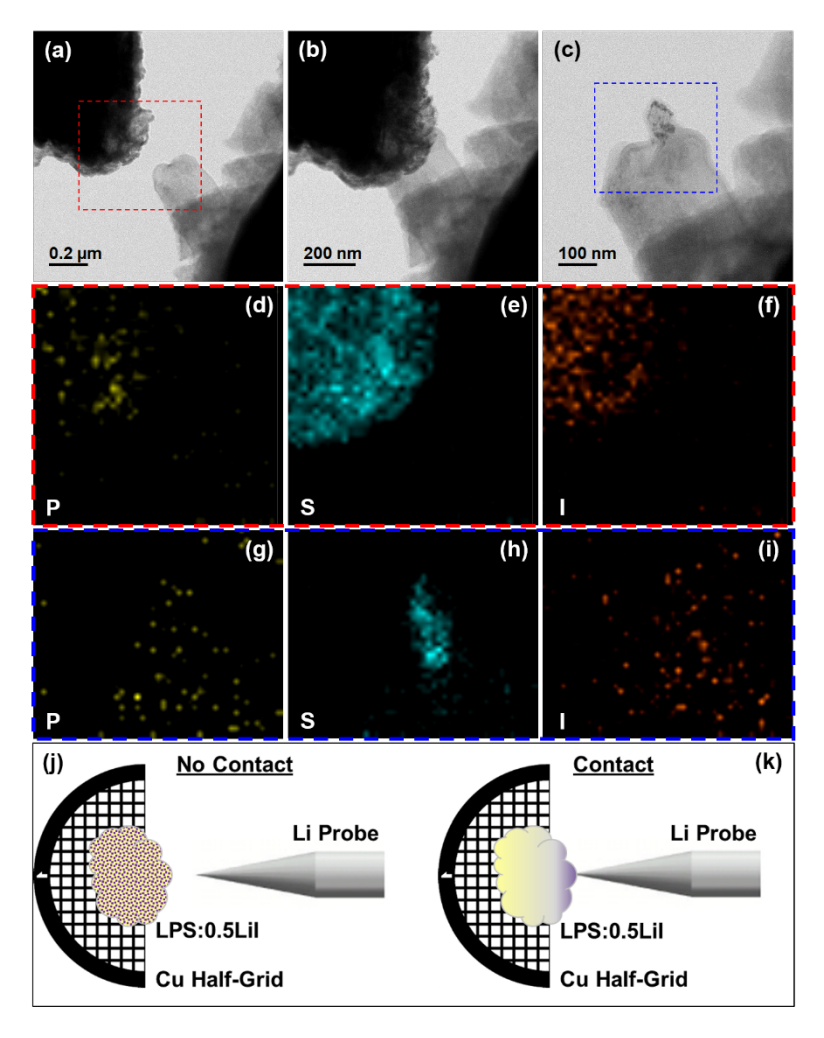


Figure 3. a)-c) TEM images of LPS:0.5LiI and a Li-metal probe pre-contact, contact and detached, respectively. d)-f) are EDS maps of P, S and I during pre-contact and g)-i) after detachment. Drawings of the TEM experiments are shown for the (j) pre-contact and (k) contact of Lithium and LPS:LiI.

results here indicate drastic differences in the interface for the deposition of lithium metal, and consequently, the failure of the electrochemical half-cell. We hypothesize the addition of lithium iodide to LPS provides an interfacial benefit to lithium deposition and stripping, beyond the reported increase to the bulk conductivity of the electrolyte. Firstly, the iodine plays a protective role to continuous decomposition of LPS in contact with lithium metal, and additionally, a leveling effect to the incongruent solid-solid interface between the metal electrode and solid-state electrolyte. However, in solution-based electrochemistry, iodine adsorption at the electrode interface is easily achieved through the liquid-solid interface, and the key to the solid-state electrochemistry would rely on iodine's diffusion and adsorption to the lithium metal surface.

The interface between lithium metal and the solid electrolyte, essential for ion transport, metal crystallization and electron impedance, must be considered chemically, morphologically and electrically to achieve the rigorous battery targets. Analysis of the interface

between LPS / LPS:0.5LiI and lithium metal was initiated by observing the surface of the solid electrolyte after densification at 4 tons cm⁻² (Figure 2a,b). As shown by the inset, the particle size of the solid electrolyte powders before densification were 1-5 µm in size. At the high-molding pressure of 4 tons/cm⁻² without the application of heat, 92% and 95 % densification of the LPS and LPS:0.5LiI pellets, respectively, can be achieved. Relative density results highlight the improved low-molding pressure densification upon LiI addition (Figure S2). Pore-size analysis of each solid electrolyte is shown in Figure 2c,d and it was found that the pore density found on the surface LPS:0.5LiI is only 73% of the pores found in LPS, however the size dispersion of the pores on the surface follow similar trends. Interestingly, the surface of the LPS:0.5LiI solid electrolyte also exhibits a smoother morphology with the less porosity, which improves the mechanical contact with the surface of the copper electrode during galvanic deposition. As shown through the investigation of the surface chemistry (vide infra), the improved interfacial contact afforded by LiI addition is only part of the reason for the improved deposition of lithium.

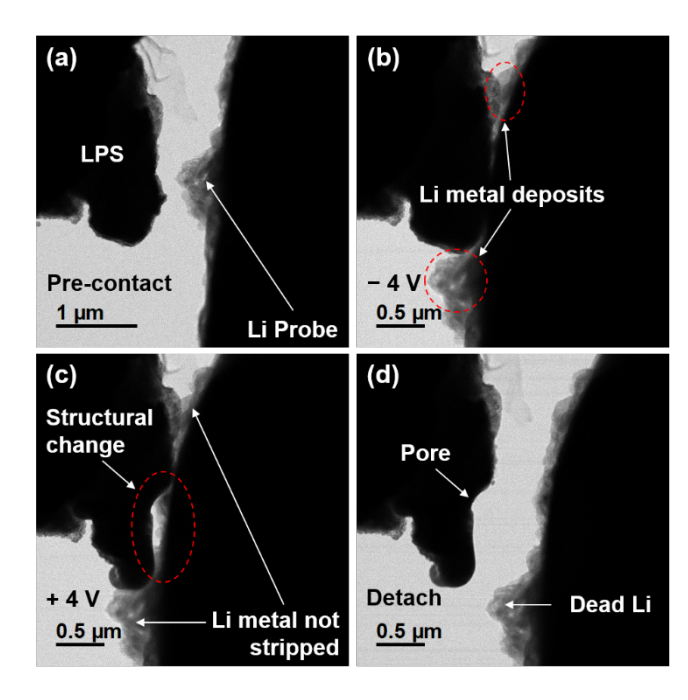


Figure 4. TEM images of Li probe and LPS a) pre-contact, *operado* electrochemical b) deposition, c) stripping and d) after detachment.

Lithium metal is a powerful chemical reductant, and multiple researchers have shown the decomposition of LPS and other lithium tiophosphates in contact with lithium metal. However, the self-limiting nature of the formation of Li₂S, Li₂S_x, and Li₃P has permitted the continued galvanic cycling, albeit under "unlimited" lithium metal cycling conditions. Previously, we have shown that the decomposition extends to LPS: 0.5LiI solid electrolyte¹¹. The addition of LiI to LPS does not completely inhibit the decomposition of the Li₃PS₄ structure after galvanic cycling, as the presence of a reduced species is observed in the XPS S2p region (Figure S3). Here, we investigated the changes to the interface of the LPS:0.5LiI solid electrolyte in contact with lithium metal for 12 h. As shown in Figure 2e, chemical diffusion of iodine to the surface of lithium metal is evidenced through XPS depth profiling. The atomic percentage of iodine and sulfur is calculated by the peak area of the I3d and S2p region, respectively. The atomic concentration of iodine, with respect to sulfur, at surface of the as-made pellet is 15.5 %, which is slightly above the theoretical nominal value 11.1 % for LPS:0.5LiI. The segregation of LiI to the surface of the LPS particles during compaction has been hypothesized by Tatsumisago et al.; LiI diffusion is responsible for the improved densification by facilitating particle-to-particle bonding in LPS:0.5LiI powder compaction.9 After 2 minutes of Ar⁺ sputtering, the atomic concentrations for the bulk pellets reflect the theoretical values for LPS:0.5LiI. By fabricating the electrochemical symmetrical Li-Li cell and maintaining an open-circuit voltage (OCV) for 12 h, the surface species of the solid electrolytes transforms into an iodine rich surface. The concentration of iodine is 74.1 % after 2 minutes of Ar+ sputtering and decreases linearly to

62% after 8 minutes. By following calculation protocols outlined by Taylor, the iodine coverage on the lithium metal is estimated to be $0.08\,\mathrm{ML}$ (ML = monolayers) 25 . This analysis is clear evidence for the diffusion and adsorption of iodine to the interface between the solid electrolyte and lithium metal. The effect of iodine surface adsorbates on the electrodeposition of metals has been previously studied, and generally, has been shown to play a protective against unwanted reactions at the electrode surface to produce compact metal deposits. Visualization of this process would establish iodine's pivotal interfacial role in the deposition of lithium metal.

Transmission electron microscopy (TEM) is established as an essential visualization tool for nanoscale materials and reactions. *Operando* experiments are quickly becoming ubiquitous and accessible to visualize and characterize important scientific processes.^{26,27} The

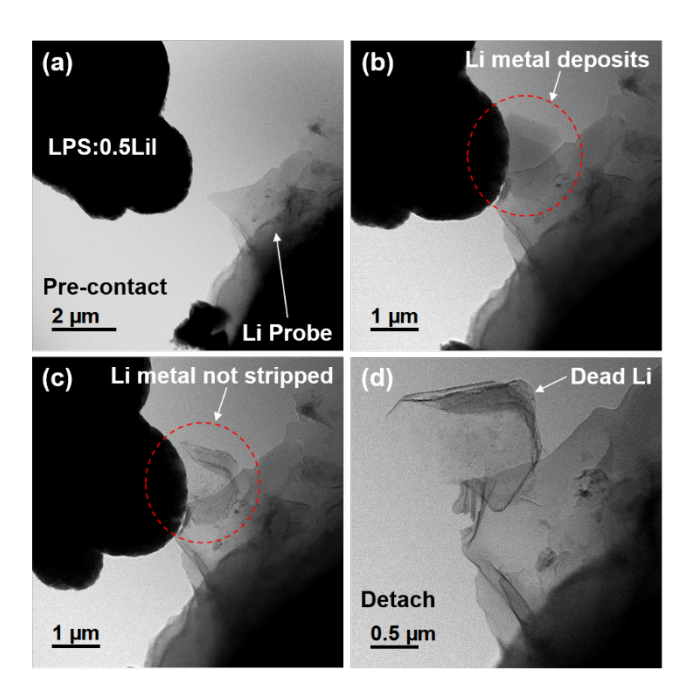


Figure 5. TEM images of Li probe and LPS:0.5LiI a) pre-contact, operado electrochemical b) deposition, c) stripping and d) after detachment.

first step to using TEM for lithium thiophosphate electrolytes is confirmation of the stability of the electrolyte in the electron microscope. Indeed, the morphology LPS and LPS:0.5LiI can be altered unless the conditions for sample preparation and the electron microscope itself are not carefully controlled (Supporting Experimental). In Figure S4, we evidence the structural stability of the LPS:0.5LiI under the time-frame needed to capture an image and perform EDS analysis with accurate quantitative yield. The solid-state chemical diffusion of iodine to the surface of LPS:0.5LiI upon contact with lithium metal prompted our TEM investigation using a nanomanipulator holder, as described in the experimental section. This technique allows for controlled contact between two materials; the solid electrolyte stabilized on a Cu TEM half-grid, and a lithium metal chunk attached to a metal probe. In Figure 3, we show the TEM

images and EDS maps of the LPS:0.5LiI and lithium metal after contact for 1 h. The pre-contact, contact and detachment images in Figure 3a-c), respectively, were analyzed for chemical composition using EDS. The analyses clearly confirms the chemical diffusion of iodine to the surface of lithium metal upon contact with the LPS:0.5LiI electrolyte (Figure 3i). The spatial location of iodine is also not found to be limited to the solid-solid contact area made between the lithium metal and solid electrolyte. As shown in Figure 3g-i), iodine diffusion is observed along the entire surface of lithium metal upon contact with LPS:0.5LiI, implying that iodine diffuses along the entire interface of lithium metal and the solid-electrolyte, irrespective of direct physical contact at a specific location. Such pronounced surface diffusion will aid to mitigate fluctuations in resistance across the electrochemical interface, resulting in a smooth voltage response to the galvanic deposition. Additionally, establishing physical contact between lithium metal and the solid electrolyte is the last step needed to drive a current within the TEM nanomanipulator holder.

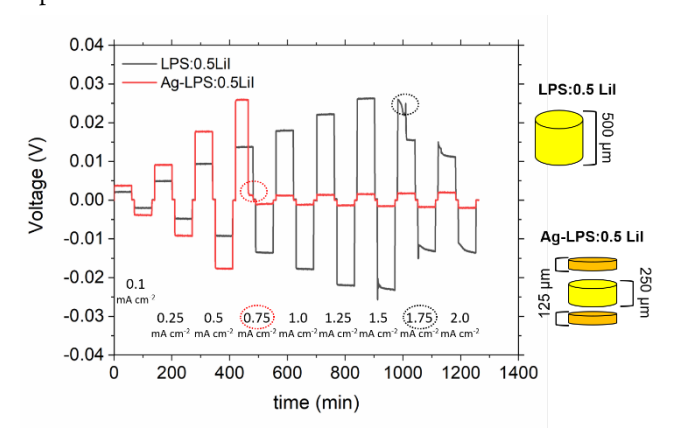
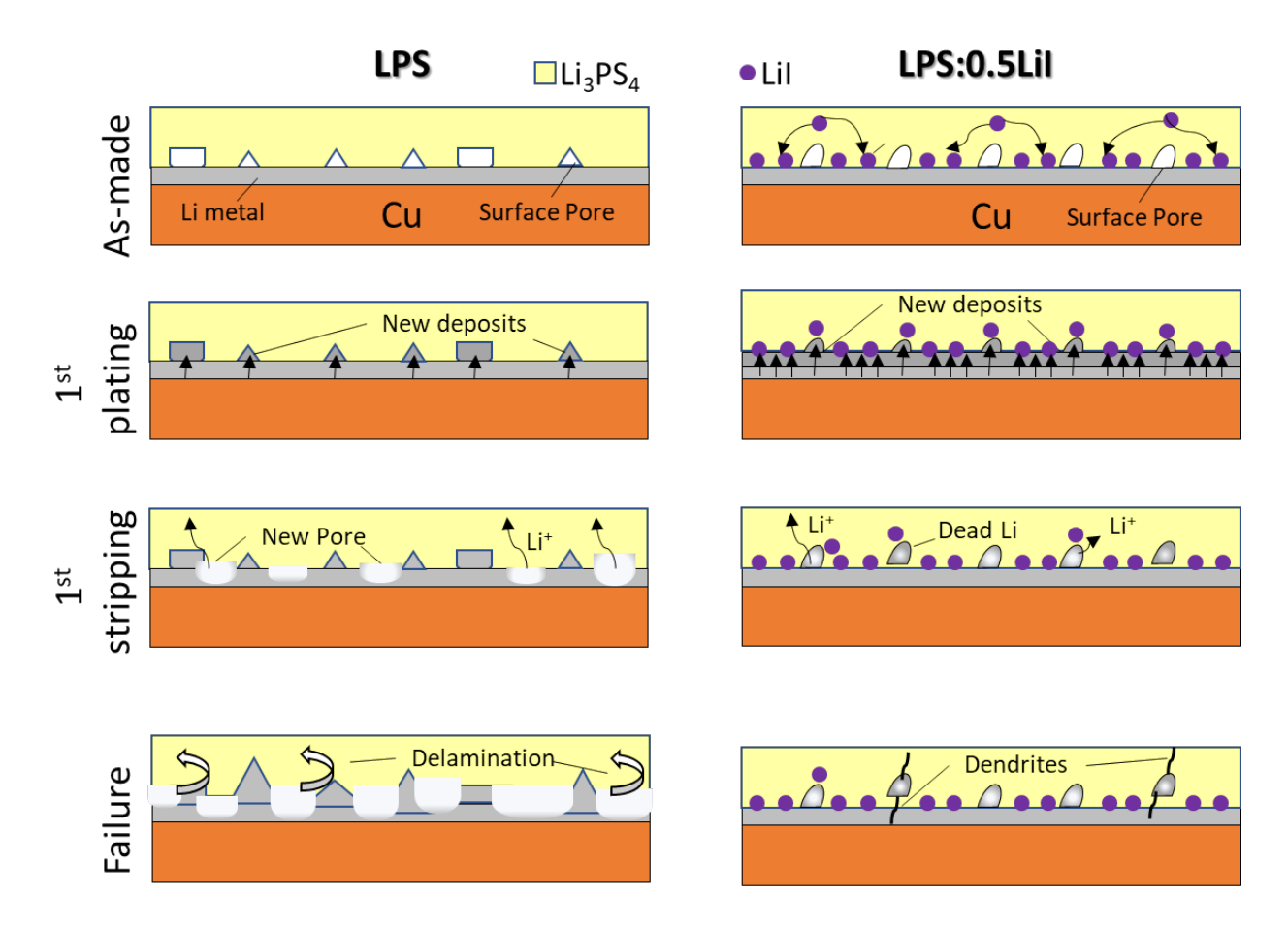


Figure 6. CCD measurements for LPS:LiI and Ag-doped LPS:LiI.

The ability to transport ions in the solid state, as well as the ability to manipulate an electrical circuit within the TEM instrument, is ideal to enact operando electrochemical-TEM as a tool to image the morphological changes in the solid electrolyte under a potential bias. In Figure 4a-d), TEM images of the LPS-Li metal interface pre-contact, -4 V (reductive plating), +4 V (oxidative stripping) and after detachment, respectively. Upon application of a negative potential, lithium metal plating is observed *surrounding* the physical interface. This result echoes the results of Sharafi et al. which shows the preferential growth of lithium metal along the grain boundaries and pores of a solid electrolyte using SEM.²⁸ However, upon application of a stripping potential, lithium metal is removed from the contact area within the physical interface, developing a pore along the electrochemical interface. Figure 5a-d) shows the TEM images of the LPS:0.5LiI-Li metal interface pre-contact, -2 V (reductive plating), +2 V (oxidative stripping) and lithium metal after detachment, respectively.



Scheme 1. Failure mechanisms for lithium deposition from LPS and LPS:0.5LiI.

Similar to LPS, lithium metal is visualized in the area *surrounding* the contact area, however as opposed to LPS, the lithium deposited lithium metal remains active and is capable of being stripped when a reversed, positive potential is applied to the interface. As Figure 5d) highlights, LPS:0.5LiI still suffers from the presence of dead lithium at the interface. Importantly, void formation is not observed in LPS:0.5LiI, a significant result showing the mechanically robust interface formed with lithium metal.

The asymmetrical locations which lithium metal plating and stripping occurs from LPS leads to multiple possible detriments for the solid-state interface: low coulombic efficiency for plating and stripping of lithium metal, porous interfacial contact between lithium metal and LPS increase the effective current density by lowering the surface area of contact, mechanical stress induced upon the bulk electrolyte through volume changes at the interface, and delamination of the solid electrolyte from the current collector surface. All these challenges must be solved, however, the mechanical delamination of the solid electrolyte from the surface of the copper current collector is likely the reason for the loss of plating capacity of observed in Figure 1b). The addition of LiI to LPS provides a softer interface for lithium metal plating, adsorption of iodine molecules

for chemical protection and electrochemical leveling, and the capability to absorb the volume changes due to lithium plating and stripping. However, the observation of "dead" lithium metal upon the initial electrochemical plating and stripping cycle points to a dynamic LPS:0.5LiI-Li metal interface which evolves with each additional plating and stripping cycle. After repeated cycling, the accrual of detached lithium particles dispersed in the ceramic matrix could alter the electrical conductivity of the interphase. One probative example is the effect of metallic nanoparticles dispersed in the interface of the LPS:LiI and lithium metal on critical current density. To mimic the effect of dead lithium at the interface, metallic silver nanoparticles (AgNPs) were doped at 1 mol % and physically dispersed into the LPS:0.5LiI interfacial layer. Figure 6 shows the cell configurations using AgNPs-doped LPS:0.5LiI (tri-layer) and LPS:LiI (single layer) and CCD results for lithium metal plating and stripping. The CCD was decreased from 1.75 mA/cm² to 0.75 mA/cm² with the addition of AgNPs. The resistance to electron flow at the interface has been decreased, which has recently shown to be a detriment to dendrite formation in SSB.29

An analytical approach to understand the interfacial differences found between LPS and LPS:0.5LiI was undertaken in this study.

Scheme 1 summarizes the findings pictorially to display the deposition and stripping process for lithium metal from the solid-electrolytes. The As-made image depicts a smooth deposition of lithium metal, below the CCD, to form a thin lithium electrode. The surface pores of LPS have sharp boundaries, while diffusion of LiI to the surface of Li₃PS₄ upon compaction produce smoother surface pore morphology. Importantly, LiI diffusion to the surface of Li-metal also occurs when contacted to lithium metal. During the first plating step, lithium metal preferentially deposits into the pores of LPS. Due to the protective and leveling abilities of iodine, lithium metal deposits more uniformly across the interface with LPS:0.5LiI. In LPS, new pores formed at the interface with lithium metal upon the initial galvanic stripping step decreases the solid-solid contact area between the anode and solid electrolyte. The asymmetric process continues until the growth of excess lithium and new pore formation delaminates the surface of lithium metal from the solid electrolyte, leading to an inability to deposit the lithium required for plating and cell failure. In contrast, LPS:0.5LiI can extract deposited lithium with a high coulombic efficiency and without detrimental morphological changes to the interface. However, pore filling and electrical detachment lead to remnant lithium at the interface. Cell failure, in this case, is caused by an increase in the interfacial electrical conductivity and subsequent dendritic growth, leading to an electrical short. The critical step to realizing lithium metal batteries in the solid state is to eliminate the presence of dead lithium after galvanic stripping.

The presence of lithium iodide in lithium thiophosphates provides key mechanical and electrochemical benefits for solid-state batteries. After achieving bulk ionic conductivities to rival commercialized liquid electrolytes, solving the issues to realize practical solid-state batteries relies on intelligent engineering of the solid-solid interfaces. To realize lithium metal as an anode, continued understanding and analysis of the interface will reveal the key challenges. The continuous improvement of *operando* visualization techniques, specifically electron microscopy, accelerates fundamental discoveries towards solid-state batteries.

ASSOCIATED CONTENT

Supporting Information. Experimental and supplementary figures. This material is available free of charge via the Internet at http://pubs.acs.org

AUTHOR INFORMATION

Corresponding Author

* Email: tim.arthur@toyota.com.

Present Addresses

1Toyota Motor Corporation, 1Toyota-cho, Toyota, Aichi 471-8572, Japan

Author Contributions

The manuscript was written through contributions of all authors. All authors have given approval to the final version of the manuscript.

Funding Sources

The authors declare no funding sources.

Notes

The authors declare no competing interests.

ACKNOWLEDGMENT

The authors would like to acknowledge Masafumi Nose and Keita Niitani for their support and encouraging discussions.

REFERENCES

- 1. Famprikis, T.; Canepa, P.; Dawson, J. A.; Islam, M. S.; Masquelier, C., Fundamentals of inorganic solid-state electrolytes for batteries. *Nat. Mater.* **2019**, Ahead of Print.
- 2. Manthiram, A.; Yu, X.; Wang, S., Lithium battery chemistries enabled by solid-state electrolytes. *Nat. Rev. Mater.* **2017**, *2*(3), 16103.
- 3. Schnell, J.; Guenther, T.; Knoche, T.; Vieider, C.; Koehler, L.; Just, A.; Keller, M.; Passerini, S.; Reinhart, G., All-solid-state lithium-ion and lithium metal batteries paving the way to large-scale production. *J. Power Sources* **2018**, *382*, 160-175.
- 4. Bachman, J. C.; Muy, S.; Grimaud, A.; Chang, H.-H.; Pour, N.; Lux, S. F.; Paschos, O.; Maglia, F.; Lupart, S.; Lamp, P.; Giordano, L.; Shao-Horn, Y., Inorganic Solid-State Electrolytes for Lithium Batteries: Mechanisms and Properties Governing Ion Conduction. *Chem. Rev.* (Washington, DC, U. S.) 2016, 116 (1), 140-162.
- 5. Kanno, R.; Murayama, M., Lithium ionic conductor thio-LISICON: the Li2S-GeS2-P2S5 system. *J. Electrochem. Soc.* **2001**, *148*(7), A742-A746.
- 6. Kamaya, N.; Homma, K.; Yamakawa, Y.; Hirayama, M.; Kanno, R.; Yonemura, M.; Kamiyama, T.; Kato, Y.; Hama, S.; Kawamoto, K.; Mitsui, A., A lithium superionic conductor. *Nat. Mater.* **2011,** *10* (9), 682-686
- 7. Park, K. H.; Bai, Q.; Kim, D. H.; Oh, D. Y.; Zhu, Y.; Mo, Y.; Jung, Y. S., Design Strategies, Practical Considerations, and New Solution Processes of Sulfide Solid Electrolytes for All-Solid-State Batteries. *Adv. Energy Mater.* **2018**, *8*(18), n/a.
- 8. Mercier, R.; Malugani, J. P.; Fahys, B.; Robert, G., Superionic conduction in lithium sulfide-phosphorus sulfide-lithium iodide glasses. *Solid State Ionics* **1981**, *5*, 663-6.
- 9. Kato, A.; Yamamoto, M.; Sakuda, A.; Hayashi, A.; Tatsumisago, M., Mechanical Properties of Li2S-P2S5 Glasses with Lithium Halides and Application in All-Solid-State Batteries. *ACS Appl. Energy Mater.* **2018**, *1* (3), 1002-1007.
- 10. Han, F.; Yue, J.; Zhu, X.; Wang, C., Suppressing Li Dendrite Formation in Li2S-P2S5 Solid Electrolyte by LiI Incorporation. *Adv. Energy Mater.* **2018**, *8*(18), n/a.
- 11. Bonnick, P.; Niitani, K.; Nose, M.; Suto, K.; Arthur, T. S.; Muldoon, J., A high performance all solid state lithium sulfur battery with lithium thiophosphate solid electrolyte. *J. Mater. Chem. A* **2019**, Ahead of Print.
- 12. Garcia-Mendez, R.; Mizuno, F.; Zhang, R.; Arthur, T. S.; Sakamoto, J., Effect of Processing Conditions of 75Li2S-25P2S5 Solid Electrolyte on its DC Electrochemical Behavior. *Electrochim. Acta* **2017**, *237*, 144-151.
- 13. Wenzel, S.; Sedlmaier, S. J.; Dietrich, C.; Zeier, W. G.; Janek, J., Interfacial reactivity and interphase growth of argyrodite solid electrolytes at lithium metal electrodes. *Solid State Ionics* **2018**, *318*, 102-112.
- 14. Wenzel, S.; Weber, D. A.; Leichtweiss, T.; Busche, M. R.; Sann, J.; Janek, J., Interphase formation and degradation of charge transfer kinetics between a lithium metal anode and highly crystalline Li7P3S11 solid electrolyte. *Solid State Ionics* **2016**, *286*, 24-33.
- 15. Albertus, P.; Babinec, S.; Litzelman, S.; Newman, A., Status and challenges in enabling the lithium metal electrode for high-energy and low-cost rechargeable batteries. *Nat. Energy* **2018**, $\mathcal{J}(1)$, 16-21.
- 16. Audrieth, L. F.; Nelson, H. W., Electrodeposition of metals from nonaqueous solvents. *Chem. Rev. (Washington, DC, U. S.)* **1931,** *8*, 335-52.
- 17. Gamburg, Y. D.; Zangari, G., *Theory and Practice of Metal Electrodeposition*. 1 ed.; Springer-Verlag New York: New York, 2011.
- 18. Hubbard, A. T., Electrochemistry at well-characterized surfaces. *Chem. Rev.* **1988**, *88* (4), 633-56.
- 19. Solomun, T.; Schardt, B. C.; Rosasco, S. D.; Wieckowski, A.; Stickney, J. L.; Hubbard, A. T., Studies of electrodeposition of silver on an iodine-pretreated stepped surface: platinum(S)[$6(111) \times (111)$]. *J. Electroanal. Chem. Interfacial Electrochem.* **1984**, 176(1-2), 309-23.

- 20. Shue, C.-H.; Yau, S.-L., In Situ Scanning Tunneling Microscopy of Underpotential Deposition of Copper at Pt(100) Electrodes Coated with an Iodine Monolayer. *J. Phys. Chem. B* **2001**, *105* (23), 5489-5496.
- 21. Liu, J.; Lei, J.; Magtoto, N.; Rudenja, S.; Garza, M.; Kelber, J. A., The effects of an iodine surface layer on Ru reactivity in air and during Cu electrodeposition. *J. Electrochem. Soc.* **2005**, *152* (2), G115-G121.
- 22. Bjelkevig, C.; Kelber, J., Stability of iodine on ruthenium during copper electrodeposition and its effects on the nucleation behavior of electrodeposited copper. *Electrochim. Acta* **2009**, *54*(15), 3892-3898.
- 23. Kim, M. J.; Kim, H. C.; Kim, J. J., The Influences of Iodide Ion on Cu Electrodeposition and TSV Filling. *J. Electrochem. Soc.* **2016**, *163* (8), D434-D441.
- 24. Ujiie, S.; Inagaki, T.; Hayashi, A.; Tatsumisago, M., Conductivity of 70Li2S-30P2S5 glasses and glass-ceramics added with lithium halides. *Solid State Ionics* **2014**, *263*, 57-61.
- 25. Taylor, A., Practical surface analysis, 2nd edn., vol I, auger and X-ray photoelectron spectroscopy. Edited by D. Briggs & M. P. Seah, John Wiley, New York, 1990, 657 pp., price: £86.50. ISBN 0471 92081 9. *Journal of Chemical Technology & Biotechnology* **1992**, *53* (2), 215-215.
- 26. Singh, N.; Arthur, T. S.; Tutusaus, O.; Li, J.; Kisslinger, K.; Xin, H. L.; Stach, E. A.; Fan, X.; Mohtadi, R., Achieving High Cycling Rates via In Situ Generation of Active Nanocomposite Metal Anodes. *ACS Appl. Energy Mater.* **2018**, *1* (9), 4651-4661.
- 27. Fan, Z.; Zhang, L.; Baumann, D.; Mei, L.; Yao, Y.; Duan, X.; Shi, Y.; Huang, J.; Huang, Y.; Duan, X., In Situ Transmission Electron Microscopy for Energy Materials and Devices. *Adv. Mater. (Weinheim, Ger.)* **2019**, *31* (33), n/a.
- 28. Cheng, E. J.; Sharafi, A.; Sakamoto, J., Intergranular Li metal propagation through polycrystalline Li6.25Al0.25La3Zr2O12 ceramic electrolyte. *Electrochimica Acta* **2017**, *223*, 85-91.
- 29. Han, F.; Westover, A. S.; Yue, J.; Fan, X.; Wang, F.; Chi, M.; Leonard, D. N.; Dudney, N. J.; Wang, H.; Wang, C., High electronic conductivity as the origin of lithium dendrite formation within solid electrolytes. *Nat. Energy* **2019**, *4*(3), 187-196.

The role of lithium iodide addition to lithium thiophosphate: Implications beyond conductivity

Nikhilendra Singh † , James Horwath ‡ , Patrick Bonnick † , Koji Suto $^{\dagger 1}$, Eric Stach ‡ , Tomoya Matsunaga $^{\dagger 1}$, John Muldoon † and Timothy S. Arthur *†

†Toyota Research Institute of North America, 1555 Woodridge Ave, Ann Arbor, MI 48105

 ‡ Singh Center for Nanotechnology, 3231 Walnut Street, Philadelphia, PA 19104

Solid-state batteries, Interface, Operando Analysis

Supporting Information

- I. Experimental Section
- II. Figures

I. Experimental

To protect the electrolyte from air, all of the below procedures were conducted under an Ar gas atmosphere with < 0.1 ppm O_2 and H_2O , either inside a glove box or within sealed experimental vessels.

Synthesis of Li₃PS₄

Anhydrous Li₂S (Aldrich, 99.98%) and anhydrous P_2S_5 (Sigma-Aldrich, 99%) to form a mixture (2.0 g total) containing a molar ratio of Li₂S: $P_2S_5 = 3:1$. This mixture was ground by hand for 5 minutes and then transferred to a 45 mL ZrO₂ ball-mill pot along with 32 g of ZrO₂ balls (5 mm diameter). The mixture was ball-milled for 40 hours using a planetary ball mill (Pulverisette 7, Fritsch). Afterward, the yellow (Li₃PS₄) powder was collected.

Synthesis of Li₃PS₄:0.5LiI electrolyte and AgNPs-doped Li₃PS₄

Anhydrous LiI beads (Aldrich, 99.999%) were added to an agate mortar and pulverized. Then, LiI was moved to a new mortar along with anhydrous Li_2S and anhydrous P_2S_5 to form a mixture (2.0 g total) containing a molar ratio of $Li_2S: P_2S_5: LiI = 3:1:1$. This mixture was ground for 5 minutes and then transferred to a 45 mL ZrO_2 ball-mill pot along with 32 g of ZrO_2 balls (5 mm diameter). The mixture was ball-milled for 40 hours using a planetary ball mill (Pulverisette 7, Fritsch). Each cycle consisted of spinning the pot for 1 h at 550 rpm and then resting the pot for 5 min. Afterward, the amorphous $Li_3PS_4\cdot 0.5LiI$ (light yellow) powder was collected and annealed at 185 °C for 3 hours. 1 mol% Silver nanoparticles (Sigma, 99.5%, < 100 nm) were added to an agate mortar and ground with LPS:0.5LIi to give AgNP-doped LPS:0.5LiI.

Scanning Electron Microscopy (SEM) / Energy Dispersive X-ray Spectroscopy (EDS)

SEM images were collected using a JEOL 7800 FLV microscope outfitted with an Oxford EDS system, operated at 5-20 kV for all samples.

Transmission Electron Microscopy (TEM) / Energy Dispersive X-ray Spectroscopy (EDS)

TEM images were collected using a JEOL JEM-F200 microscope operated at 200 kV. Dual silicon-drift detector EDS systems with a large solid angle (100 mm²) were utilized for enhanced microanalysis of all samples via ex-situ and in-situ analysis modes.

- Specific to ex-situ TEM: All samples for ex-situ analysis were loaded onto 3 mm 300-mesh lacy carbon coated copper grids (Ted Pella) within an Argon atmosphere glove box (< 0.1 ppm O₂ and H₂O). The loading was carried out by directly scooping the grid through the sample material

contained within a glass vial. As such, this was a dry-casting method and no solvents were utilized during the process at any time to prevent possible reactions between sample materials and solvents. The materials cast and analyzed using this process were Li₃PS₄ and Li₃PS₄:0.5LiI. In addition to general imaging and elemental analysis, ex-situ TEM was utilized as a benchmark to establish the necessary microscope settings (e.g. probe size, beam current, spot size, exposure time, etc.) to successfully image and analyze the materials without damage from the beam itself. It should be noted that each material is expected to have different behavior under the beam and as such should be benchmarked prior to in-situ TEM analysis efforts to ensure an optimized setup.

- Holder designed by Hummingbird Scientific. The holder assembly was carried out within an Argon atmosphere glove box (< 0.1 ppm O₂ and H₂O). This in-situ holder utilized a 3mm 300-mesh lacy carbon coated copper half-grid (Ted Pella) and a tungsten (W) scanning tunneling microscopy (STM) probe (Bruker). The biasing capability of the in-situ holder allowed for the application and observation of a current and/or voltage between the half-grid and STM probe. The movable STM probe could be brought into contact with the half-grid to complete a circuit and conduct electrochemistry experiments within the TEM. Below, we provide a description of how the in-situ holder was setup for the experiments highlighted in this manuscript:
 - O The holder was brought into the glove box using standard protocols and the holder tip was disassembled within the glove box to separate components for the half-grid and the probe. Specific tools (procured from Hummingbird Scientific) for the holder were also brought into the glove box to ensure damage-free disassembly/assembly of the holder.
 - Half-grid: For all experiments, Li₃PS₄ or Li₃PS₄:0.5LiI materials were loaded onto the half-grid using the procedure described for ex-situ TEM. The material loaded half-grid was then assembled into the holder component designed for the half-grid.
 - o STM Probe: The W probe was converted into a lithium (Li) coated W probe for our applications, as follows. Li metal foil (MTI Corporation) was first cleaned by mechanical scraping of the foil surfaces using the plastic cap of a standard 20 ml glass vial (VWR). This scraped Li foil piece was placed on top of a 100-micron thick nickel (Ni) foil (Alfa Aesar) which was contained within a glass petri dish (VWR). The petri dish, along with the Ni and Li foil materials were then heated until the Li was observed to melt at which point the W probe was very gently dipped into the molten Li to procure the Li coated W probe. The dipping was accomplished by bringing the molten Li into contact with the probe, not vice-versa, to ensure safety of the fragile probe.

- The holder was now completely reassembled within the glove box and the holder tip (containing the material loaded half-grid and Li probe components) was secured for air-free transfer from the glove box by using a customized air-free holder cap. Once secure with this cap, the holder was removed from the glove box using standard protocols and immediately moved to the TEM for loading.
- The holder was loaded into the TEM while the air-lock for the TEM holder vented either nitrogen or argon gas to ensure air-free entry of the holder into the TEM. The custom air-free holder cap was removed from the holder at the TEM point of entry immediately prior to loading the holder into the TEM and pumping it down instantly to minimize sample exposure to air during this process.

Once the holder was pumped down in the TEM, a suitable Li₃PS₄ or Li₃PS₄:0.5LiI sample was located on the edge of the half-grid closest to the Li probe, and the Li probe was moved into position to contact this sample using manual and electronic adjustments to the probe via Hummingbird Scientific software. Upon contact, the noted experiments in the manuscript were carried out using a Bio-Logic SP-200 Potentiostat.

X-ray Photoelectron Spectroscopy (XPS)

X-ray photoelectron spectroscopy (XPS) was collected using a PHI 5000 Versaprobe II and analyzed using the Multipack software. Spectra were aligned to the C1s signal at 284.7 eV. Ar⁺ sputtering was performed at an energy of 2 kV for an allotted time.

Conductivity measurement

100 mg of Li₃PS₄·0.5LiI powder was added to the hole in a Macor ring (SA = 1.0 cm²) and cold-pressed between two steel pistons into a pellet under 4 tons of pressure for 5 min. Then, carbon-coated aluminum foil (MTI corp.) disks were placed against both sides of the pellet and the stack was pressed again under 3 tons for about 1 min. After removing the stack from the press, the pistons were anchored in place by a cell top and bottom, held together by insulated bolts. The bolts were tightened to 2 N·m, which provides a stack pressure of about 88 MPa. Finally, the cell was sealed in an argon-filled container and placed into a temperature-controlled oven. Electrochemical impedance spectroscopy was performed using a Bio-logic VMP3 potentiostat, with a frequency range from 100 mHz to 1 MHz and a potential amplitude of 10 mV. The electrolyte resistance was determined from the EIS plots by extrapolating the low-frequency, linear section of the curves down to the x-axis.

Fabrication of Cu/SE/Li Half cells.

100 mg of solid electrolyte powder was added to the hole in a Macor ring and cold-pressed between two steel pistons under 4 tons of pressure for 5 min to form a pellet. Then a 1 cm² piece of copper foil (Aldrich, 0.25 mm) was added to one side and the stack was pressed again under 3 tons for about 1 min. Separately, a thick Li disk (99.8%, Honjo Metal) of 10 mm diameter was polished with a toothbrush then punched from the flattened Li using a knife punch, which were then placed against the opposite side of the pellet from the Cu foil. Stainless-steel pistons were pressed against the Cu and Li to form a stack, which was then sandwiched between cell top and bottom. Finally, insulated bolts were used to compress the cell to 29 MPa before placing the cell into an argon-filled container, which was then moved from the glove box to an oven for electrochemical testing.

Fabrication of Li/SE/Li symmetric cells.

For LPS:0.5LiI measurements, 100 mg of LPS:0.5LiI was added to the hole in a Macor ring and cold-pressed between two steel pistons under 4 tons of pressure for 5 min to form a pellet. For AgNP-doped measurements, 50 mg of LPS:0.5LiI was pressed under 4 tons of pressure, followed by the addition of 25 mg of AgNP-doped LPS:0.5LiI to either side of the pellet. Then the stack was pressed again at 4 tons of pressure for 5 minute to form a tri-layer pellet. Then a thick Li disk (99.8%, Honjo Metal) of 10 mm diameter was polished with a toothbrush then punched from the flattened Li using a knife punch, which were then placed on both sides of the pellet. Stainless-steel pistons were pressed against the Li to form a stack, which was then sandwiched between cell top and bottom. Finally, insulated bolts were used to compress the cell to 29 MPa before placing the cell into an argon-filled container, which was then moved from the glove box to an oven for electrochemical testing.

Critical Current Density (CCD) test.

Li metal was plated and stripped at step-wise-increased current densities using a Bio-logic VMP3 potentiostat. At 60°C, the current density was increased in a stepwise manner from 0.1 mA/cm² to 2.0 mA/cm² in 0.25 mA/cm² steps. Each current was applied using 1-hour half-cycles for 2 cycles. The CCD was ascribed to the current at which a sharp drop in potential was witnessed mid-half-cycle.

II. Figures

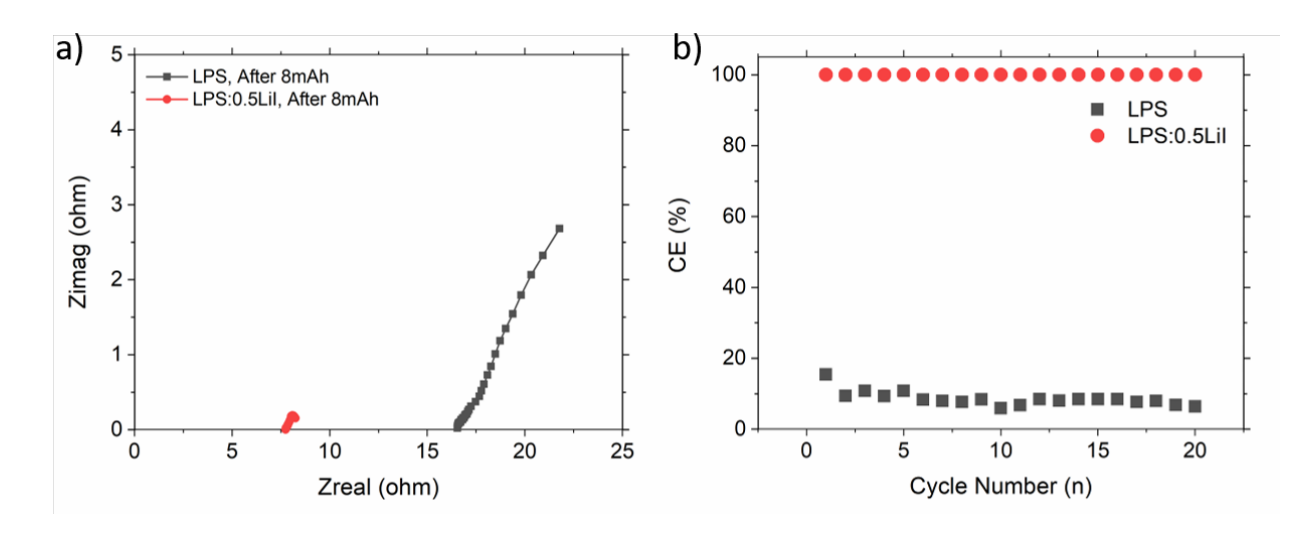


Figure S1. a) EIS of Cu/SE/Li halr-cells after 8 mAh of galvanic lithium plating at 0.25 mA cm $^{-2}$. b) Coulombic Efficiency (CE), defined as ($Q_{stripping}/Q_{plating}$), of Cu/Se/Li half-cells at 1 mA cm $^{-2}$ for 1 mAh.

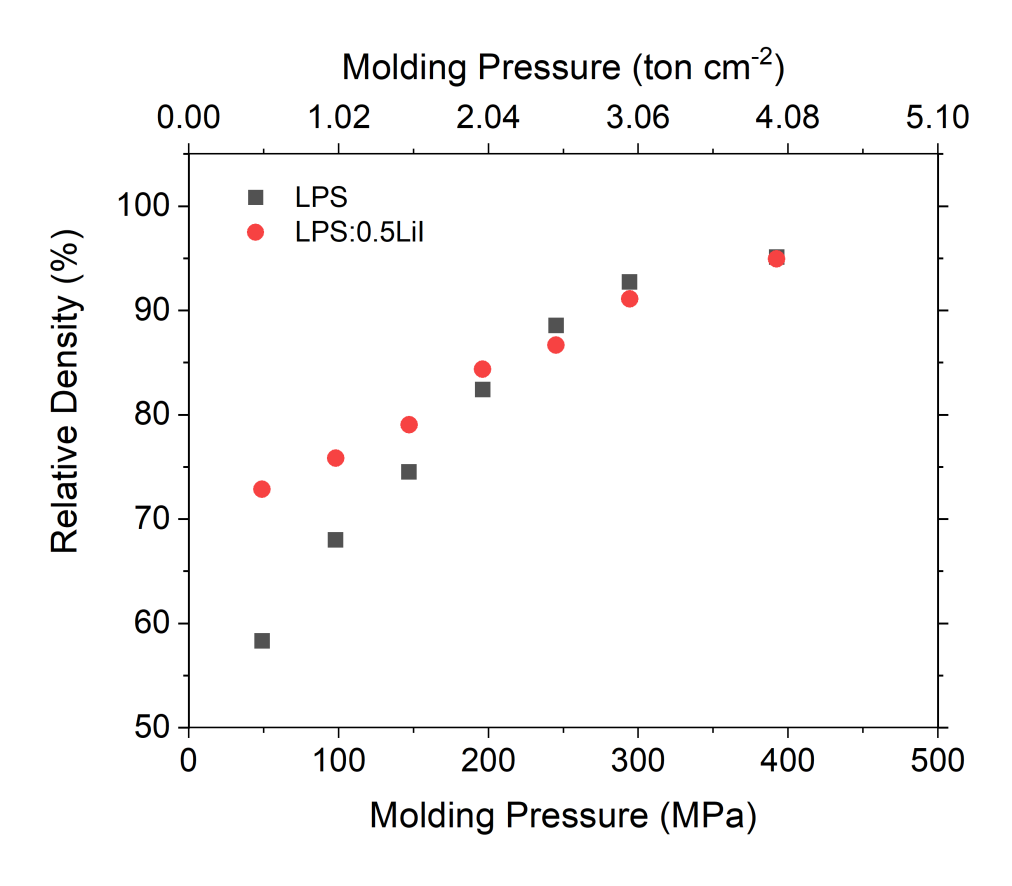


Figure S2. a) Relative Density of pelletized solid electrolytes under increasing molding pressure.

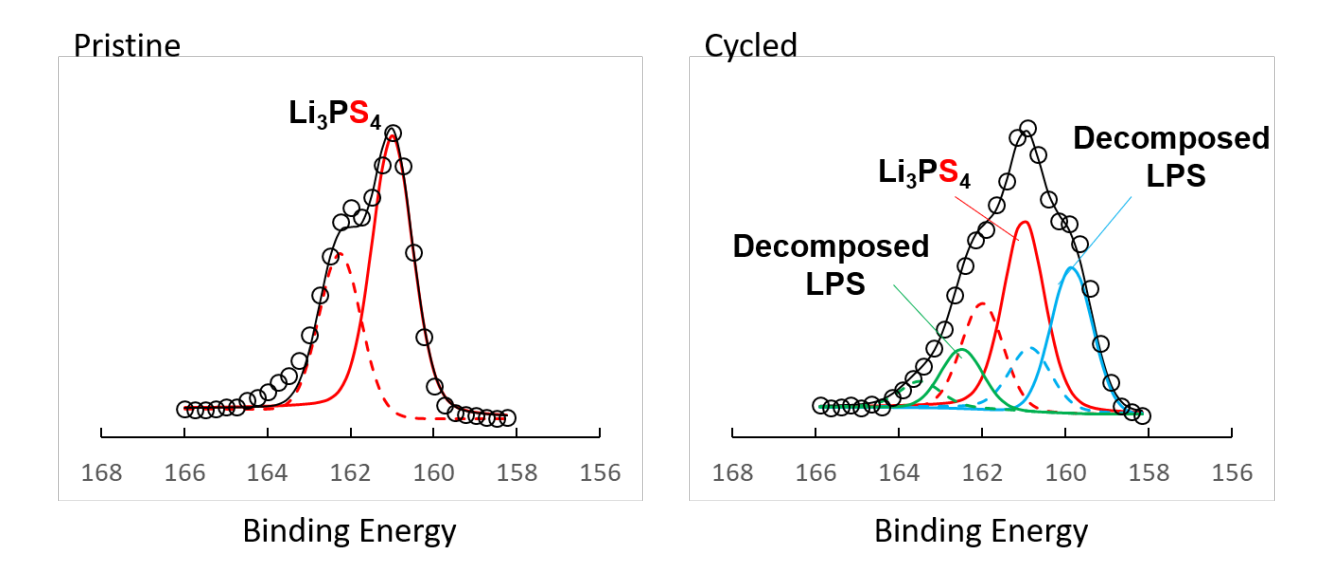


Figure S3. S2p XPS spectra and de-convolution of LPS:0.5LiI as a Pristine pellet and after galvanic cycling with lithium metal.

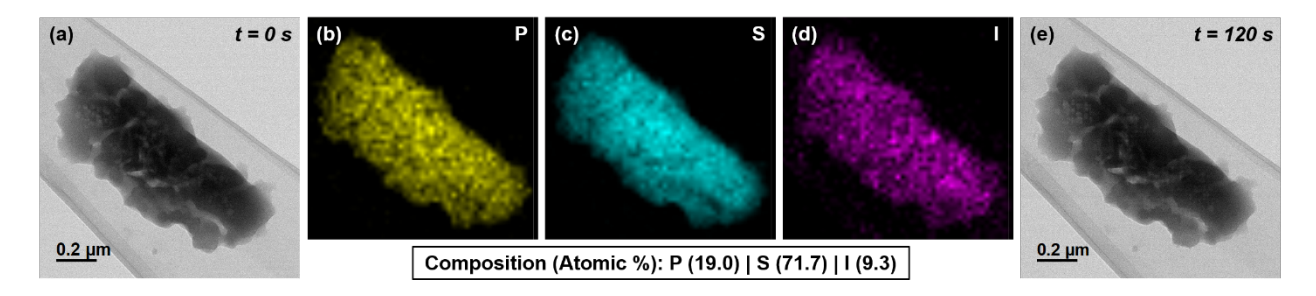


Figure S4. LPS:0.5LiI stability is shown for 120 s in a transmission electron microscope.